# Fractional-order poromechanics for a fully saturated biological tissue: Biomechanics of meniscus

Received: 2 January 2023 | Revised: 17 April 2023 | Accepted: 27 April 2023

DOI: 10.1002/cnm.3732

SPECIAL ISSUE ARTICLE

WILEY

# Fractional-order poromechanics for a fully saturated biological tissue: Biomechanics of meniscus

**Fabiana Amiri**[1] | **Emanuela Bologna**[1,2] | **Gianmarco Nuzzo**[1] | **Lorenzo Moroni**[3] | **Massimiliano Zingales**[1,2]

[1]Department of Engineering, University of Palermo, Palermo, Italy

[2]Bio/NanoMechanics for Medical Sciences Laboratory (BNM 2-Lab), Advanced Technology Network (ATeN)-Center, CHAB Pole, Palermo, Italy

[3]Complex Tissue Regeneration Department, MERLN Institute for Technology-inspired Regenerative Medicine, Maastricht University, Maastricht, Netherlands

**Correspondence**
Emanuela Bologna, Department of Engineering, University of Palermo, Viale delle Scienze ed. 8 90128, Palermo, Italy.
Email: emanuela.bologna@unipa.it

**Funding information**
PON FSE-FESR ricerca e innovazione, Grant/Award Number: 2014-2020DOT1320558; Ricercatori a tempo Determinato tipo A (RTDA), Grant/Award Number: 20-I-39045-8; SiciliAn MicronanOTecH Research And Innovation CEnter SAMOTHRACE, Grant/Award Numbers: ECS00000022, PNRR-M4C2; S2-COMMs-Micro and Nanotechnologies for Smart & Sustainable Communities

## Abstract

Biomechanics of biological fibrous tissues as the meniscus are strongly influenced by past histories of strains involving the so-called material hereditariness. In this paper, a three-axial model of linear hereditariness that makes use of fractional-order calculus is used to describe the constitutive behavior of the tissue. Fluid flow across meniscus' pores is modeled in this paper with Darcy relation yielding a novel model of fractional-order poromechanics, describing the evolution of the diffusion phenomenon in the meniscus. A numerical application involving an 1D confined compression test is reported to show the effect of the material hereditariness on the pressure drop evolution.

**KEYWORDS**
fractional calculus, fractional-order hereditariness, meniscus, pore pressure, poromechanics

## 1 | INTRODUCTION

Meniscus is C-shaped fibro-cartilaginous tissues situated between femoral condolences and tibia. They perform many important biomechanical functions, such as shock absorption and uniform load distribution, co-operate with tendons and protect the knee joint from damage by hyper-extension and hyper-flexion. They also play a critical role in the proprioception, lubrication of joints and nutrition of articular cartilage.[1,2] The complete or partial loss of a meniscus can have negative effects on the knee, resulting in serious long-term consequences. Several studies have been conducted to formulate menisci mechanical behavior, but this is extremely difficult due to their complex inhomogeneous microstructure and lack of comprehensive experimental characterization of material properties.[3–6]

In recent years, a considerable number of studies have been conducted on poroelastic models to describe diffusion phenomenon on meniscus.[7–9] In these models, Fick and/or Darcy transport equations has been modified using fractional calculus in order to introduce the memory effect induced by the interaction of fluid particles and pore structure of the elastic medium.[10,11] In other studies, a power-law variation of the geometric and physical properties of the porous medium was considered, leading to a fractional-order relationship between incoming flow and pressure applied to the control section.[12] The common base of aforementioned approaches is represented by the linear elastic behavior of the fibrous tissue representing the meniscus. However, it is well-known as

  

reported in relevant scientific literature that the stress in collagen tissue representing meniscus depends on past history of strain and not only on the actual value of the strain.[13–17] This effect is known as *material hereditariness* and it is usually represented by coupling linear elastic springs and linear viscous dashpot to represent the material behavior.[11,18–22]

In this study, the authors use the fractional-order hereditariness model to describe the mechanical behavior of fibrous tissue by means of a three axial model. Indeed, experimental behavior of meniscal tissues in long-standing uniaxial test is represented by Creep function $J(t)$ and Relaxation function $G(t)$ that may be modeled as power-law $J(t) \propto t^{\beta}$ and $G(t) \propto t^{-\beta}$ with $0 \leq \beta \leq 1$, yielding an accurate description of experimental data.[3,18,23–26] The numerical examples discussed in the paper involves a confined compression test in a semi-drained condition and a fully drained test that have been used in order to exploit the constitutive relation of the investigated model. It has been shown that the biomechanics of the proposed model is markedly influenced by three parameters, namely the anomalous consolidation coefficients $C_{\alpha}$ and $C_{\beta}$, accounting for different deformation effects and the $\beta$ order of Caputo's fractional-order derivative. The governing equations of the poromechanical problem of the fractional hereditary materials (FHM) were obtained and solved as for the case of cylindrical symmetry. In particular, the classic 1D confined compression test and fully drained test of a poromechanics are studied, using the classical poroelasticity for comparison's sake. In the conclusions, the authors highlight how, also in this application, the effects of Caputo's fractional derivative well describe the problem when the order of the $\beta$ derivation varies. In particular, the physical meanings of the chosen ranges of $\beta$ values are analyzed and explained.

## 2 | THE CONSTITUTIVE EQUATIONS OF FRACTIONAL-ORDER POROMECHANICS

The presence of a biphasic material containing, respectively, a fluid and a solid component is usually faced in the context of elastic behavior of the solid and fully viscous behavior,[2,3] with very low Reynolds numbers, of the fluid. The representative volume elements (RVE), namely the smallest volume that contains elements of the solids and pores filled by fluid phase involved in poromechanics contains at the same time the two phases that interacts only in the force balance conditions and that undergoes the same strain field. As a consequence the constitutive equations of poromechanics requires, besides the six relations among the six components of the stress vector in and the six components of the strain vector in Voigt representation the additional hydrostatic stress field $p(t)$, omitting spatial dependence, that represent variation of pressure in the fluid phase. This latter additional state variable is paired by the balance of fluid content rate $\dot{\zeta}(t)$ that, however needs the knowledge of the fluid flux across the boundaries of the reference volume. Darcy equation for the diffusive motion of the fluid is therefore used to model fluxes in terms of the material permeability, a measure of the interconnection of the material pores allowing for fluid motion.

The presence of biological tissues with a marked presence of hydrated collagen, as in meniscus tissue, makes, however, largely ineffective the elastic models of the material since a marked-time dependent behavior of the representative volume element is observed also in absence of fluid-filling material pores.[13,16,27–34] As a consequence a mathematical formulation that can be used to represent this mechanical behavior is the linear theory of material hereditariness that is nowadays described by the so-called Fractional-Order hereditariness (FOH). In this setting the formalism of fractional-calculus, lately used in several biomechanical contexts[18,21,25,26] allows to replace the well-known constitutive equations of classical linear elasticity with their-fractional-order counterparts, involving, as additional parameters the derivation order $\beta \in [0,1]$. In this section, we introduces, shortly, the basic equation of FHM in uniaxial case (2.1), as well as in the three-axial case (2.2), and, subsequently, the constitutive relation for a biphasic material (2.3).

### 2.1 | Long-standing uniaxial tests in FHM

The presence of material hereditariness is usually detected for linear material behavior, where this time-dependent behavior is expressed in terms of creep and relaxation function. In detail, $J(t)$ denotes the strain response to the unit step of stress (Creep test), while $G(t)$ denotes the stress response to a unit step of strain (Relaxation test). Moreover, by

using the Boltzmann superposition principle, the general stress–strain relation can be expressed in terms of one material function [J(t) or G(t)] through a linear hereditary integral[11,19]:

$$\sigma(t) = \int_0^t G(t-\sigma)d\varepsilon(\sigma) = \int_0^t G(t-\sigma)\dot{\varepsilon}(\sigma)d\sigma, \tag{1a}$$

$$\varepsilon(t) = \int_0^t J(t-\sigma)d\sigma(\sigma) = \int_0^t J(t-\sigma)\dot{\sigma}(\sigma)d\sigma, \tag{1b}$$

Where $[\cdot] = \frac{d}{dt}$, so $d\sigma = \dot{\sigma}dt$ and $d\varepsilon = \dot{\varepsilon}dt$. Additionally, creep and relaxation function must satisfy the reciprocity relation in the Laplace domain:

$$\widehat{J}(s)\widehat{G}(s) = \frac{1}{s^2}, \tag{2}$$

$s$ indicates the Laplace parameter and $\widehat{f}(s) = \mathcal{L}[f(t)]$ is the Laplace transform of the generic function $f(t)$.

In the context of materials hereditariness, a power-law representation of creep and relaxation functions was introduced in the early twentieth century,[20] that is:

$$G(t) = \frac{C_\beta t^{-\beta}}{\Gamma(1-\beta)}, \tag{3a}$$

$$J(t) = \frac{t^\beta}{C_\beta \Gamma(\beta+1)}, \tag{3b}$$

where $\Gamma$ is the Euler-Gamma function, while $\beta \in [0,1]$ and $C_\beta > 0$ are material parameters, that may be estimated through a best-fitting procedure of experimental data.[21,35,36]

Furthermore, substituting Equations (3a) and (3b) into Equations (1a) and (1b), it is found that the constitutive laws for linear FHM are ruled by fractional operator:

$$\sigma(t) = \frac{C_\beta}{\Gamma(1-\beta)} \int_0^t (t-\sigma)^{-\beta}\dot{\varepsilon}(\sigma)d\sigma = C_\beta \left({}_0^C\mathcal{D}_t^\beta \varepsilon\right)(t), \tag{4a}$$

$$\varepsilon(t) = \frac{1}{C_\beta \Gamma(\beta+1)} \int_0^t (t-\sigma)^{\beta}\dot{\sigma}(\sigma)d\sigma = \frac{1}{C_\beta}\left({}_0\mathcal{I}_t^\beta \sigma\right)(t), \tag{4b}$$

where ${}_0^C\mathcal{D}_t^\beta$ is the so-called Caputo fractional derivative, which is a generalization of an integro-differential operator of integer order, while ${}_0\mathcal{I}_t^\beta$ is the Riemann-Liouville fractional integral, with $0 < \beta < 1$. Due to the fact that, as $\beta$ tends to 0 or 1, zero and first order derivatives are respectively obtained, Equations (4a) and (4b) reduce to the constitutive law of a purely elastic material (a spring) or a Newton-Petroff purely viscous fluid (a dashpot), respectively.[1,37] So, Equations (4a) and (4b) essentially indicate that any linear viscoelastic material has an intermediary behavior between an elastic material and a viscous material. Consequently, use of power-laws and of fractional-order operators is usually connected to the introduction of the so-called springpot element in the rheological context.[38]

## 2.2 | Three-axial constitutive equations of FHM

The extension of the constitutive relation presented in Section 2.1 to the more general case of three axial isotropic material is shortly discussed in this section. The three-axial state of stress in an FHM is described by the 2nd-order stress

tensor $\sigma$ with component $\sigma_{ij}$ which presents the symmetries $\sigma_{ij}=\sigma_{ji}$ for $i\neq j$ and $i,j=1,2,3$. In the same way, the state of strain is described, by the 2nd-order small strain tensor $\varepsilon$.

Particularly, in this paper we use vector description of the state variables of the material introducing the six-component stress and strain vectors, respectively as:

$$\sigma^T(t)=[\sigma_{11}(t)\sigma_{22}(t)\sigma_{33}(t)\sigma_{32}(t)\sigma_{31}(t)\sigma_{12}(t)], \tag{5a}$$

$$\varepsilon^T(t)=[\varepsilon_{11}(t)\varepsilon_{22}(t)\varepsilon_{33}(t)\varepsilon_{32}(t)\varepsilon_{31}(t)\varepsilon_{12}(t)], \tag{5b}$$

where $t$ is the current time, while $\sigma_{ij}(t)$ and $\varepsilon_{ij}(t)$ are the mixed index stress and strain components, namely $i\neq j$ denote shear stress and strain, respectively.

Let us assume that $\sigma_{ij}(t)=\sigma_{ij}(t)\delta_{ij}$, where $\delta_{ij}$ is the well-known Kronecker symbol that is $\delta_{ij}=0$ when $i\neq j$ and equals to 1 for all other cases, namely $i=j$; consequently, let us consider a single normal stress $\sigma_{ii}=1$ for $(i=1,2,3)$.

In such a context, the evolution of the strain $\varepsilon_{ii}(t)$ both along the stress direction $\sigma_{ii}(t)$ and in the orthogonal planes reads:

$$\varepsilon_{ii}(t)=J_L(t)\sigma_{ii}=J_L(t), \tag{6a}$$

$$\varepsilon_{kk}(t)=\varepsilon_{jj}(t)=-J_v(t)\sigma_{ii}, \tag{6b}$$

with $i\neq j\neq k$ and $i,j,k=1,2,3$. In Equations (6a), (6b) $J_L(t)$ and $J_v(t)$ are the axial and the transverse creep functions with respect to the stress direction, respectively. Under the assumption of smooth load process $\sigma_{ij}(t)$ with $i=1,2,3$, the presence of contemporaneous stress may be accounted for by the integral:

$$\varepsilon_{ii}(t)=\int_0^t J_L(t-\sigma)\dot{\sigma}_{ii}(\sigma)-J_v(t-\sigma)\left[\dot{\sigma}_{jj}(\sigma)+\dot{\sigma}_{kk}(\sigma)\right]d\sigma. \tag{7}$$

In the context of material isotropy, shear strains $2\varepsilon_{ij}(t)$ (with $i\neq j$) are not involved by the axial stress $\sigma_{ii}(t)$, but only by the shear stress as $\sigma_{ij}(t)$ with $i\neq j$. The evolution of the shear strain $2\varepsilon_{ij}(t)$ due to a generic shear stress history $\sigma_{ij}(t)$ may be obtained by superposition integrals by means of the shear creep function $J_T(\cdot)$ as:

$$2\varepsilon_{ij}(t)=\int_0^t J_T(t-\sigma)\dot{\sigma}_{ij}(\sigma)d\sigma \tag{8}$$

with $i\neq j$ and $i,j=1,2,3$. The constitutive equations reported in Equations (7), (8) may be reported in Voigt notation as:

$$\varepsilon(t)=\int_0^t \mathbf{J}(t-\sigma)\dot{\sigma}(\sigma)d\sigma, \tag{9}$$

where $\mathbf{J}(t)$ is the creep functions matrix that is described as:

$$\mathbf{J}(t)=\begin{bmatrix}\mathbf{J}^{(A)}(t) & \mathbf{0}\\ \mathbf{0} & \mathbf{J}^{(T)}(t)\end{bmatrix}, \tag{10}$$

$\mathbf{J}^{(A)}(t)$ includes the elements of the axial creep matrix that is:

$$J_{ij}^{(A)}(t) = J_L(t)\delta_{ij} - \left(1-\delta_{ij}\right)J_v(t), \tag{11}$$

While $\mathbf{J}^{(T)}(t)$ is the shear creep matrix, which is a diagonal matrix gathering the shear creep functions $J_T(t)$ as:

$$J_{ij}^{(T)}(t) = J_T(t)\delta_{ij}. \tag{12}$$

Particularly, the three creep functions $J_L(t)$, $J_v(t)$ and $J_T(t)$ are related by a linear relation that reads[12]:

$$J_T(t) = 2J_L(t) - J_v(t). \tag{13}$$

As seen in Equation 2, creep function matrix $\mathbf{J}(t)$ in Equation (10) is related to the definition of the relaxation matrix $\mathbf{G}(t)$ by means of the conjugation relation as:

$$\widehat{\mathbf{G}}(s)\widehat{\mathbf{J}}(s) = \frac{1}{s^2}\mathbf{I}, \tag{14}$$

where $\mathbf{I}$ is the identity matrix, while $\widehat{G}(s)$ and $\widehat{J}(s)$ are the Laplace transforms of the relaxation $\mathbf{G}(t)$ and creep $\mathbf{J}(t)$ functions matrices, respectively.

With straightforward manipulations of Equation (14), the relaxation matrix may be written as:

$$\mathbf{G}(t) = \begin{bmatrix} \mathbf{G}^{(A)}(t) & \mathbf{0} \\ \mathbf{0} & \mathbf{G}^{(T)}(t) \end{bmatrix}, \tag{15}$$

where:

$$G_{ij}^{(A)}(t) = \mathcal{L}^{-1}\left[\frac{1}{s^2\left(\widehat{J}_L+\widehat{J}_v\right)\left(\widehat{J}_L-2\widehat{J}_v\right)}\right]\left[\left(\widehat{J}_L-\widehat{J}_v\right)\delta_{ij} + \left(1-\delta_{ij}\right)\widehat{J}_v\right], \tag{16a}$$

$$G_{ij}^{(T)}(t) = \mathcal{L}^{-1}\left[\frac{1}{s^2\left(\widehat{J}_L+\widehat{J}_v\right)}\right]\delta_{ij}. \tag{16b}$$

Boltzmann superposition principle, allows, therefore to the evaluation of the stress vector that reads:

$$\boldsymbol{\sigma}(t) = \int_0^t \mathbf{G}(t-\sigma)\dot{\boldsymbol{\varepsilon}}(\sigma)d\sigma. \tag{17}$$

The torsional, longitudinal and transverse relaxation functions $G_T(t)$, $G_L(t)$, and $G_v(t)$ are linearly related by an equation that is similar to the one involving creep functions in Equation (13), reading[12]:

$$G_T(t) = \frac{1}{2}(G_L(t) - G_v(t)). \tag{18}$$

The latter allows for the evaluation of the transverse relaxation $G_v(t)$, as:

$$G_v(t) = G_L(t) - 2G_T(t) \tag{19}$$

Introducing the power-law representation of the relaxation matrix $\mathbf{G}(t)$ into Equation (17) as:

$$\mathbf{G}(t) = \mathbf{G}_\beta \frac{t^{-\beta}}{\Gamma(1-\beta)} + \overline{\mathbf{G}} \tag{20}$$

with the coefficient matrices:

$$\mathbf{G}_\beta = \begin{bmatrix} G_\beta^{(L)} & G_\beta^{(\upsilon)} & G_\beta^{(\upsilon)} & 0 & 0 & 0 \\ G_\beta^{(\upsilon)} & G_\beta^{(L)} & G_\beta^{(\upsilon)} & 0 & 0 & 0 \\ G_\beta^{(\upsilon)} & G_\beta^{(\upsilon)} & G_\beta^{(L)} & 0 & 0 & 0 \\ 0 & 0 & 0 & G_\beta^{(T)} & 0 & 0 \\ 0 & 0 & 0 & 0 & G_\beta^{(T)} & 0 \\ 0 & 0 & 0 & 0 & 0 & G_\beta^{(T)} \end{bmatrix}, \tag{21a}$$

$$\overline{\mathbf{G}} = \begin{bmatrix} \overline{G}_L & \overline{G}_\upsilon & \overline{G}_\upsilon & 0 & 0 & 0 \\ \overline{G}_\upsilon & \overline{G}_L & \overline{G}_\upsilon & 0 & 0 & 0 \\ \overline{G}_\upsilon & \overline{G}_\upsilon & \overline{G}_L & 0 & 0 & 0 \\ 0 & 0 & 0 & \overline{G}_T & 0 & 0 \\ 0 & 0 & 0 & 0 & \overline{G}_T & 0 \\ 0 & 0 & 0 & 0 & 0 & \overline{G}_T \end{bmatrix}. \tag{21b}$$

It yields a relation between the stress vector and the history of the strain vector $\varepsilon(t)$ as:

$$\boldsymbol{\sigma}(t) = \mathbf{G}_\beta \int_0^t (t-\sigma)^{-\beta} \dot{\boldsymbol{\varepsilon}}(\sigma) d\sigma + \overline{\mathbf{G}} = \mathbf{G}_\beta \left( \mathcal{D}_{0^+}^\beta \varepsilon \right)(t) + \overline{\mathbf{G}}. \tag{22}$$

The stress vector obtained as a functional of the strain vector $\varepsilon(t)$ in Equation (22) is the generalization of the constitutive equation reported in Equation (4a) under the assumption of material isotropy.

Moreover, in the following discussion we assume that $\overline{\mathbf{G}} = \mathbf{0}$, so that a simplified expression for the inverse constitutive equation corresponding to Equation (22) is obtained:

$$\boldsymbol{\varepsilon}(t) = \mathbf{J}_\beta \int_0^t (t-\sigma)^{\beta-1} \boldsymbol{\sigma}(\sigma) d\sigma = \mathbf{J}_\beta \left( \mathcal{I}_{0^+}^\beta \boldsymbol{\sigma} \right)(t), \tag{23}$$

where $\mathbf{J}_\beta = \mathbf{G}_\beta^{-1}$ is the creep-coefficient function and it plays the same role as the compliance matrix of the linear theory of elasticity.

## 2.3 | The constitutive relation for biphasic FHM

The three-axial hereditariness presented in previous section allows for the introduction of the effects of the presence of an additional fluid phase in the material pores, as in case of meniscus. To this aim, let us consider the RVE of the meniscus and let us refer the edges to a three axial orthogonal reference system as in Figure 1.

Let us assume, in the following that the solid phase is represented by a FHM so that the constitutive relations are obtained as in Section 2.2. The presence of the fluid phase, instead is accounted for introducing an additional state variable represented by the fluid pore pressure field, namely, $p$ in the constitutive equation ruling material strains as:

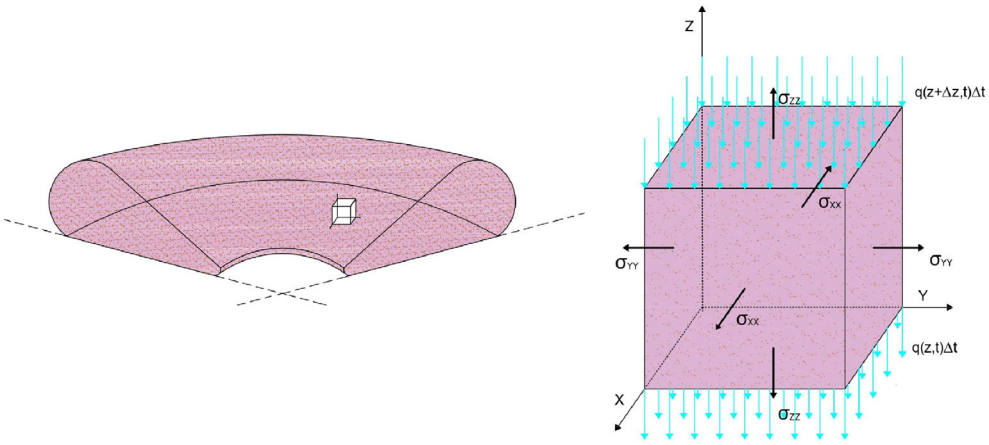


**FIGURE 1** Schematic representation of a cubic element (on the right side) extracted from the meniscus (on the left side) where the blue arrows represent the fluid flow across the cubic element, while the black arrows represent normal stresses to the surface.

$$\begin{cases} \varepsilon_{11} = J_\beta^L \mathcal{I}_t^\beta \left( \sigma_{11} - J_\beta^\nu (\sigma_{22} + \sigma_{33}) \right) + \dfrac{p}{3H} \\ \varepsilon_{22} = J_\beta^L \mathcal{I}_t^\beta \left( \sigma_{22} - J_\beta^\nu (\sigma_{11} + \sigma_{33}) \right) + \dfrac{p}{3H} \\ \varepsilon_{33} = J_\beta^L \mathcal{I}_t^\beta \left( \sigma_{33} - J_\beta^\nu (\sigma_{22} + \sigma_{11}) \right) + \dfrac{p}{3H}, \\ 2\varepsilon_{32} = J_\beta^T \mathcal{I}_t^\beta \sigma_{32} \\ 2\varepsilon_{31} = J_\beta^T \mathcal{I}_t^\beta \sigma_{31} \\ 2\varepsilon_{12} = J_\beta^T \mathcal{I}_t^\beta \sigma_{12} \end{cases} \tag{24}$$

$H$ is a bulk modulus for fluid variation pressure,[39] while $J_\beta^L, J_\beta^\nu, J_\beta^T$ are the axial, transverse and torsional component of the Creep Matrix function $\mathbf{J}_\beta$ defined in Section 2.2.

Furthermore, system Equation (24) can also be written in matrix form, as:

$$\boldsymbol{\varepsilon} = \mathbf{J}_\beta \left( {}_c\mathcal{I}_t^\beta \boldsymbol{\sigma} \right) + \frac{1}{3H} \mathbf{p}, \tag{25}$$

where $\boldsymbol{\varepsilon}$ and $\boldsymbol{\sigma}$ are the well-known strain and stress vectors of the solid, respectively. While, $\mathbf{p}$ is the fluid pressure field, defined as $\mathbf{p}^T = p[1 \;\; 1 \;\; 1 \;\; 0 \;\; 0 \;\; 0]$.

Therefore, Equation (25) expresses the six strain components of the solid as a function of stress $\sigma$ in the solid and fluid pressure $\mathbf{p}$ into the pores. In this context, the dependency of the changes of fluid content $\xi(t)$ on these variables also needs to be considered:

$$\xi(t) = \frac{1}{3H} (\sigma_{11} + \sigma_{22} + \sigma_{33}) + \frac{p}{R}, \tag{26}$$

where $R$ is a physical constant, too.[39]

In first approximation, Equations (25) and (26) completely describe the properties of solid, for strain and fluid content, under equilibrium conditions. However, it is convenient to express stress as functions of strain and fluid pressure, namely:

$$\boldsymbol{\sigma} = {}_c\mathcal{D}_t^\beta \left[ \mathbf{G}_\beta \left( \boldsymbol{\varepsilon} - \frac{1}{3H} \mathbf{p} \right) \right], \tag{27}$$

where $\mathbf{G}_\beta$ is the Relaxation Matrix Function reported in previous section (2.2).

The overall stress components in the saturated FHM may then be referred to the strain components and the fluid pressure as:

$$\begin{cases} \sigma_{11} = 2G_{\beta_c}^{T}\mathcal{D}_t^{\beta}(\varepsilon_{11}+r\theta_I)-\alpha_c\mathcal{D}_t^{\beta}p \\ \sigma_{22} = 2G_{\beta_c}^{T}\mathcal{D}_t^{\beta}(\varepsilon_{22}+r\theta_I)-\alpha_c\mathcal{D}_t^{\beta}p \\ \sigma_{33} = 2G_{\beta_c}^{T}\mathcal{D}_t^{\beta}(\varepsilon_{33}+r\theta_I)-\alpha_c\mathcal{D}_t^{\beta}p \\ \sigma_{32} = G_{\beta_c}^{T}\mathcal{D}_t^{\beta}2\varepsilon_{32} \\ \sigma_{31} = G_{\beta_c}^{T}\mathcal{D}_t^{\beta}2\varepsilon_{31} \\ \sigma_{12} = G_{\beta_c}^{T}\mathcal{D}_t^{\beta}2\varepsilon_{12} \end{cases}. \tag{28}$$

With two specific coefficients:

$$r=\frac{G_{\beta}^{\nu}}{2G_{\beta}^{T}};\quad \alpha=\frac{2G_{\beta}^{T}+3G_{\beta}^{\nu}}{3H}; \tag{29}$$

whereas, $\theta_I$ represents the volume increase of the solid per initial volume unit, namely the linear strain invariant $\theta_I=\varepsilon_{11}+\varepsilon_{22}+\varepsilon_{33}$. Although, substituting Equation (28) into Equation (26), increase in fluid content $\xi(t)$ becomes:

$$\xi(t)=\alpha_c\mathcal{D}_t^{\beta}\left[\theta_I-\frac{p}{H}\right]+\frac{p}{R}. \tag{30}$$

Its derivative is:

$$\dot{\xi}(t)=\alpha_c\mathcal{D}_t^{\beta+1}\left[\theta_I-\frac{p}{H}\right]+\frac{1}{R}\frac{\partial p}{\partial t}. \tag{31}$$

Additionally, Darcy's law, which governs water flow in the porous medium, has been introduced to complete the system:

$$\mathbf{q}=-\frac{k}{\mu}\boldsymbol{\nabla}p, \tag{32}$$

where $\mathbf{q}$ is the vector of specific volume flux across a generic cross-section, $k$ is the Darcy permeability coefficient depending on the material ($m^2$) and $\mu$ is the fluid viscosity ($kg\,m^{-1}\,s^{-1}$). Besides, assuming that water is in-compressible, the water content rate of the solid must be equal to the volume of water entering per second through the surface of the element, so:

$$\dot{\xi}(t)=-\boldsymbol{\nabla}\cdot\mathbf{q}. \tag{33}$$

Combining the last two equations:

$$\dot{\xi}(t)=\frac{k}{\mu}\boldsymbol{\nabla}^2p, \tag{34}$$

and substituting Equation (34) into Equation (31), the constitutive equation for a isotropic viscoelastic porous medium becomes:

$$\alpha_c \mathcal{D}_t^{\beta+1}\left[\theta_I - \frac{p}{H}\right] + \frac{1}{R}\frac{\partial p}{\partial t} = \frac{k}{\mu}\boldsymbol{\nabla}^2 p. \tag{35}$$

For the particular case $\beta = 0$, Equation (35) is equals to the classical poroelasticity equation that is,

$$\left[\frac{1}{R} - \frac{2a}{H}\right]\frac{\partial p}{\partial t} = \frac{k}{\mu}\nabla^2 p. \tag{36}$$

## 3 | POROMECHANICS OF A CYLINDRICALLY-SHAPED FHM

In this section, we use the constitutive Equation (35) in order to describe the settlement phenomenon that occurs into an FHM porous medium under a permanent static condition. We discuss this case introducing a symmetric cylinder in the poromechanics problem as in (Figure 2) that allows for the reduction of the kinematic field represented by the components of the displacement vector along a cylindrical reference system, namely, $u_r(r,\theta,x_3,t)$, $u_\theta(r,\theta,x_3,t)$ and $u_3(r,\theta,x_3,t)$ to just a one-dimensional component. Indeed for this case, $u_r = u_\theta = 0$ everywhere and $u_3(r,\theta,x_3,t) = w(x_3,t)$. The specimen is loaded by a constant and uniform pressure along the free surface of the cylinder $\overline{\sigma}$ and we denote the fluid pressure field as $p(x_3,t)$.

Under those circumstances, the kinematic restrictions associated to the problem reads:

$$\begin{cases} \varepsilon_{33} = \dfrac{\partial w(x_3,t)}{\partial x_3} \\ \varepsilon_{rr} = \varepsilon_{\theta\theta} = 0 \end{cases}, \tag{37}$$

so that, the first-invariant reads: $\theta_I = \varepsilon_{33} = \frac{\partial w(x_3,t)}{\partial x_3}$.

In this section, we do not consider specific boundary conditions at the top of the specimen (for $z = h$), that will be provided for two cases of semi-drained and fully drained cases in the next section. The flow across the bottom vanishes in one of the two cases ($q(z,t) = 0$ for $z = 0$), whereas vanishing overpressure is observed at the top bottom in both cases $p(h,t) = 0$ for $z = h$..

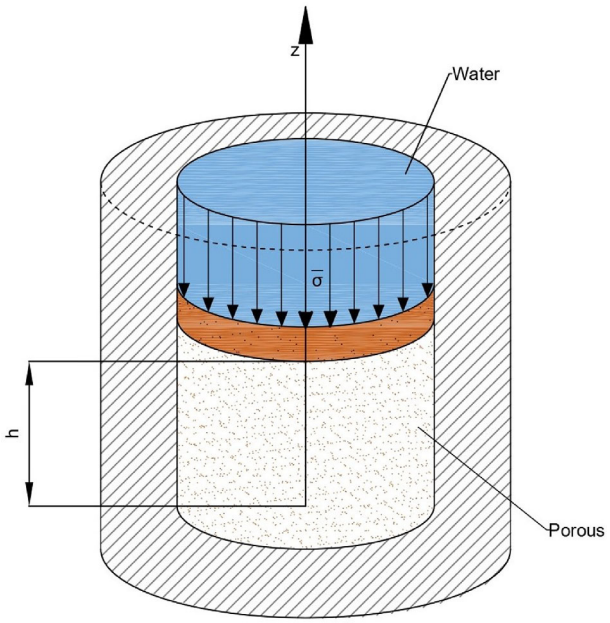


**FIGURE 2** Scheme of confined compression problem of a porous cylindrical material on which a constant pressure is imposed by a porous membrane.

In the following, simplified notation will be used introducing a $z$-axis in the direction of $x_3$ with the same origin and, therefore the vertical stress field will be denoted as $\sigma_{zz}(z,t)=\sigma_{33}(x_3,t)$.

$$\frac{\partial p(z,t)}{\partial z}=0,\quad z=0. \tag{38}$$

Consequently, differential fluid Equation (35) becomes:

$$\alpha_c \mathcal{D}_t^{\beta+1}\left[\frac{\partial w(z,t)}{\partial z}-\frac{p(z,t)}{H}\right]+\frac{1}{R}\frac{\partial p(z,t)}{\partial t}=\frac{k}{\mu}\frac{\partial^2 p(z,t)}{\partial z^2} \tag{39}$$

Supporting a load $\overline{\sigma}$ on z-axis, Equation (28) becomes:

$$\sigma_{33}=\left(2G_\beta^T+G_\beta^\nu\right)_c\mathcal{D}_t^\beta\frac{\partial w(z,t)}{\partial z}-\alpha\left({}_c\mathcal{D}_t^\beta p\right)(z,t)=-\overline{\sigma}. \tag{40}$$

Deriving Equation (40) and replacing it in Equation (39):

$$C_\beta\left({}_c\mathcal{D}_t^{\beta+1}p\right)(z,t)+C_\alpha\frac{\partial p(z,t)}{\partial t}=\frac{\partial^2 p(z,t)}{\partial z^2}. \tag{41}$$

Both $C_\alpha$ and $C_\beta$ are" anomalous" consolidation coefficients (in the sense of fractional calculus), defined as:

$$C_\beta=\frac{\alpha\mu}{k}\left(\frac{\alpha}{2G_\beta^T+G_\beta^\nu}-\frac{1}{H}\right)\quad\text{and}\quad C_\alpha=\frac{\mu}{Rk}. \tag{42}$$

Particularly, as $\beta=0$ the solid has an Elastic behavior, so the well-known consolidation equation is obtained, in 1D condition (see Eq.5.4[39]). In detail, the sum of these two coefficients returns the inverse of the so-called consolidation constant $c_v$ ($\mathrm{m2\,s^{-1}}$).

$$C_\beta+C_\alpha=\frac{1}{c_v}. \tag{43}$$

Equation (41), with initial and boundary conditions, leads to the complete solution of diffusion problem in a porous medium. In detail, this diffusion phenomenon is ruled by three parameters, namely the anomalous consolidation coefficients $C_\alpha$ and $C_\beta$, and the order of Caputo's derivative $\beta$.

In order to further reduce the number of parameters, the relation (41) can be converted into a non-dimensional form using the parameters reported below:

$$\overline{p}=\frac{p}{P_0}\quad\overline{C}_\beta=\frac{C_\beta}{\tau_c}\quad\overline{t}=\frac{t}{\tau_c}\quad\overline{z}=\frac{z}{h}. \tag{44}$$

$\overline{C}_\beta$ is the part of the anomalous consolidation coefficient, which is independent of $\beta$. Considering $\tau_c$ the characteristic time of the process and $h$ the cylinder height, $\overline{t}$ and $\overline{z}$ respectively correspond to the dimensionless values of time and space.

Consequently, the non-dimensional pressure equation is:

$$\frac{\partial}{\partial\overline{t}}\left[\overline{C}_\beta\left(\mathcal{D}_{\overline{t}}^\beta\overline{p}\right)(\overline{z},\overline{t})+\frac{C_\alpha}{\tau_c}\overline{p}(\overline{z},\overline{t})\right]=\frac{\partial^2\overline{p}(\overline{z},\overline{t})}{\partial\overline{z}^2}. \tag{45}$$

Equation (45) has been solved through variable separation method (see 2.2.1[40]), namely separating $\overline{p}(\overline{z},\overline{t})$ into non-dimensional space-dependent $\phi(\overline{z})$ and non-dimensional time-dependent $y(\overline{t})$ functions, as reported below:

$$\overline{p}(\overline{z},\overline{t}) = \phi(\overline{z})y(\overline{t}). \tag{46}$$

After substituting Equation (46) into Equation (45), a separation constant $\lambda$ has been introduced:

$$\frac{1}{\phi}\frac{d^2\phi}{d\overline{z}^2} = \frac{1}{y}\left[\overline{C}_\beta \mathcal{D}^{\beta+1}y + \frac{C_\alpha}{\tau_c}\frac{dy}{d\overline{t}}\right] = -\lambda^2. \tag{47}$$

Equation (47) is equivalent to the two following differential equations:

$$\phi''(\overline{z}) + \lambda^2\phi(\overline{z}) = 0, \tag{48a}$$

$$\overline{C}_\beta\left(\mathcal{D}^{\beta+1}y\right)(\overline{t}) + \frac{C_\alpha}{\tau_c}y'(\overline{t}) + \lambda^2 y(\overline{t}) = 0. \tag{48b}$$

The first equation is related to space-evolution, while the second one is related to time-evolution. In detail, Equation (48a) is a second order differential equation whose general solution is, for $\lambda > 0$:

$$\phi(\overline{z}) = D_1\cos(\lambda\overline{z}) + D_2\sin(\lambda\overline{z}), \tag{49}$$

Where $D_1$ and $D_2$ are two arbitrary constants, which have been evaluated through the boundary conditions. Solving the non-dimensional space $\overline{z}$ problem, then the non- dimensional time dimension has also been solved.

In particular, Laplace transform method[41–43] has been used to solve the fractional differential equation of Equation (48b)

$$Y(s) = \frac{y(0)\left[\overline{C}_\beta s^\beta + \frac{C_\alpha}{\tau_c}\right] + \overline{C}_\beta s^{\beta-1}y'(0)}{\overline{C}_\beta s^{\beta+1} + \frac{C_\alpha}{\tau_c}s + \lambda^2}. \tag{50}$$

Its inverse Laplace transform is:

$$y(\overline{t}) = \mathcal{L}^{-1}\{Y(s)\}. \tag{51}$$

Consequently, the solution is (see Eq.5.3.38[41]):

$$y(\overline{t}) = \sum_{k=0}^{\infty}\left(-\frac{\lambda_n^2}{\overline{C}_\beta}\right)^k\frac{\overline{t}^{k(\beta+1)}}{k!}E^k_{\beta,k(\beta+1)+1}\left(-\frac{C_\alpha}{\tau_c\overline{C}_\beta}\overline{t}^\beta\right) + \frac{C_\alpha}{\tau_c\overline{C}_\beta}\sum_{k=0}^{\infty}\left(-\frac{\lambda_n^2}{\overline{C}_\beta}\right)^k\frac{\overline{t}^{k(\beta+1)+\beta}}{k!}E^k_{\beta,(\beta+1)(k+1)}\left(-\frac{C_\alpha}{\tau_c\overline{C}_\beta}\overline{t}^\beta\right), \tag{52}$$

$E^k_{\beta,k(\beta+1)}$ is the three parameters Mittag-Leffler function,[44,45] defined as $E^k_{\alpha,\beta}(z) = \frac{d^k}{dz^k}E_{\alpha,\beta}(z)$, where:

$$E_{\alpha,\beta}(z) = \sum_{k=0}^{\infty}\frac{z^k}{\Gamma(\beta+\alpha k)} \tag{53}$$

with $\alpha,\beta,z \in C$ and $\Re(\alpha) > 0, \Re(\beta) > 0$. In any case, this function is commonly used to find the solution to initial value problems of a class of fractional partial differential equations.

Replacing Equations (52) and (49) into Equation (46), the general solution is:

$$\overline{p}(\overline{z},\overline{t}) = (D_1\cos(\lambda\overline{z}) + D_2\sin(\lambda\overline{z}))\sum_{k=0}^{\infty}\left(-\frac{\lambda_n^2}{\overline{C}_\beta}\right)^k\frac{\overline{t}^{k(\beta+1)}}{k!}E^k_{\beta,k(\beta+1)+1}\left(-\frac{C_\alpha}{\tau_c\overline{C}_\beta}\overline{t}^\beta\right)+ \\ +\frac{C_\alpha}{\tau_c\overline{C}_\beta}\sum_{k=0}^{\infty}\left(-\frac{\lambda_n^2}{\overline{C}_\beta}\right)^k\frac{\overline{t}^{k(\beta+1)+\beta}}{k!}E^k_{\beta,(\beta+1)(k+1)}\left(-\frac{C_\alpha}{\tau_c\overline{C}_\beta}\overline{t}^\beta\right). \tag{54}$$

In the following section numerical examples for a semi-drained condition as well as of an undrained condition will be exploited to show the effect of fluid diffusion across the pores of an FHM.

## 4 | NUMERICAL APPLICATION

In this section, the authors provide a numerical application for two particular cases: the first with initial pressure zero at $z = 0$ and the second case with pressure zero for $z = 0$ and $z = \mathrm{h}$. It must be stressed that, at the best of the authors' knowledge no experimental papers on fractional poromechanical models may be found in scientific literature but only on fractional-order darcy generalization.[7,8,11,46]

These particular cases of the fractional derivatives in Equation (45) shows the evolution of the problem for different value of $\beta$, in particular $\beta = 0{,}0.25{,}0.50{,}0.75{,}0.90{,}1$, fixing the value of the dimensionless time $\overline{t}$, as shown in Figures 3 and 6. Furthermore, it is shown that for $\beta = 0$ the remarkable cases known in the literature return[39] (Figures 3A, 6A). For this reason, the author investigated the choice of model parameters to be used to achieve steady-state flow. In detail, the input parameters of the mathematical equation are $\tau_c = 30s, \overline{C}_\beta = 7s^\beta/m^2, C_\alpha = 8\ \mathrm{s/m^2}$. The use of these values has been an arbitrary choice of the authors in order to have a qualitative representation of the fractional diffusion phenomenon.

### 4.1 | Semi-drained condition

The authors study the effect of the derivation order $\beta$ on the Equation (45) with the boundary conditions (38). Consequently, for the non-dimensional space Equation (48a)

$$\begin{cases} p(1,t) = \phi(1)y(t) = \phi(1) = 0 \\ \dfrac{\partial p(0,t)}{\partial z} = \phi'(0)y(t) = \phi'(0) = 0 \end{cases}. \tag{55}$$

It implies that $D_2 = 0$ and $\cos(\lambda) = 0 \rightarrow \lambda_n = \frac{(2n-1)\pi}{2}$; with $n = 1{,}2{,}3.....$ So Equation (49) becomes, trivial solution excluded,

$$\phi(\overline{z}) = D_1\cos(\lambda_n\overline{z}). \tag{56}$$

To satisfy initial conditions $p(z,0) = 1$, $\overline{t} = 0$ has been set, obtaining:

$$\sum_{n=1}^{\infty} D_n\cos(\lambda_n\overline{z}) = 1, \tag{57}$$

due to the fact that $\forall n \rightarrow y_n(0) = 1$.

This Sturm-Liouville series on $0 < \overline{z} < 1$ can be thought of as a Fourier cosine series on $0 < \overline{z} < 2$ for which the even-numbered cosine terms are absent.[40] The orthogonality relations has been used to determine the coefficients $D_n$:

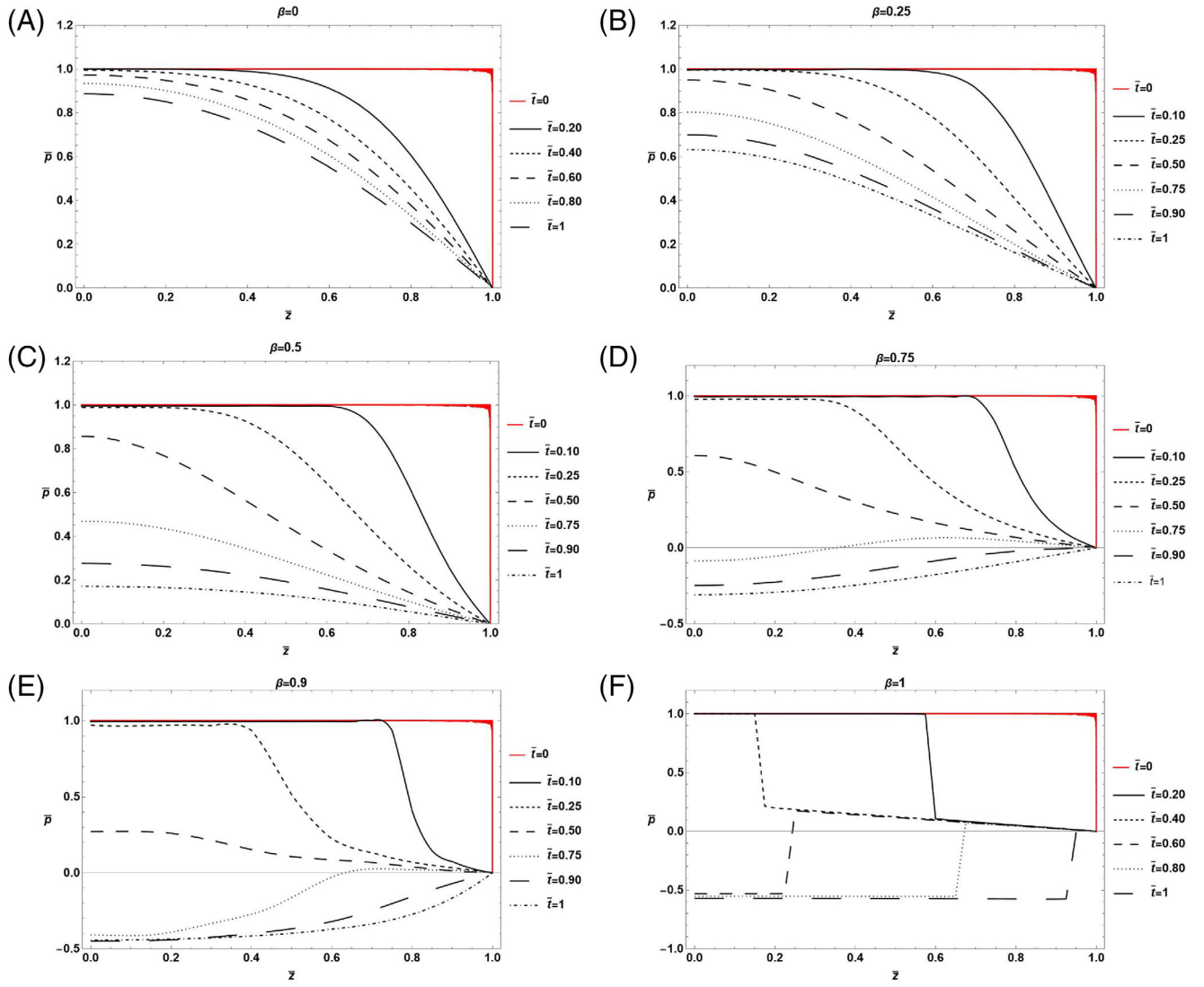


**FIGURE 3** Non-dimensional pressure field $\bar{p}$ for different values of $\beta$ in the confined compression test; particularly $\beta = 0$ (A), $\beta = 0.25$ (B), $\beta = 0.5$ (C), $\beta = 075$ (D), $\beta = 0.9$ (E), and $\beta = 1$ (F). Each curve represents the pressure field for a specific value of non-dimensional time $\bar{t}$, where the red line represents the confined compression test at the initial time $\bar{t} = 0$.

$$D_n = 2\int_0^1 \cos(\lambda_n \bar{z})\, d\bar{z} = \frac{4(-1)^n}{\pi(1-2n)}. \tag{58}$$

Therefore, the solution of the dimensionless problem is:

$$\bar{p}(\bar{z},\bar{t}) = \frac{4}{\pi}\sum_{n=1}^{\infty}\frac{(-1)^n}{1-2n}\cos(\lambda_n \bar{z})\sum_{k=0}^{\infty}\left(-\frac{\lambda_n^2}{\bar{C}_\beta}\right)^k \frac{\bar{t}^{k(\beta+1)}}{k!}E^k_{\beta,k(\beta+1)+1}\left(-\frac{C_\alpha}{\tau_c \bar{C}_\beta}\bar{t}^\beta\right) + \\ + \frac{C_\alpha}{\tau_c \bar{C}_\beta}\sum_{k=0}^{\infty}\left(-\frac{\lambda_n^2}{\bar{C}_\beta}\right)^k \frac{\bar{t}^{k(\beta+1)+\beta}}{k!}E^k_{\beta,k(\beta+1)+1+\beta}\left(-\frac{C_\alpha}{\tau_c \bar{C}_\beta}\bar{t}^\beta\right). \tag{59}$$

So, in order to shown the trend of pressure with the variation of non-dimensional $\bar{z}$-coordinate and $\bar{t}$ time, we solved Equation (59) with Wolfram Mathematica 13.1 Software (see Figure 3):

$$f_1(\beta,t,z)=\frac{4}{\pi}\sum_{n=1}^{N}\frac{(-1)^n}{1-2n}\cos\left[\frac{(2n-1)\pi z}{2}\right]\sum_{k=0}^{100}\left(-\frac{\left(\frac{(2n-1)\pi z}{2}\right)^2\tau_c{}^{\beta}}{C_\beta}\right)^k\frac{t^{(\beta+1)k}}{k!}\left(\frac{\Gamma[k+1]}{\Gamma[k(\beta+1)+1]}-\frac{C_\alpha\tau_c{}^{\beta-1}t^{\beta}\Gamma[k+2]}{C_\beta\Gamma[\beta+k(\beta+1)+1]}\right)+$$
$$+\left(-\frac{\left(\frac{(2n-1)\pi z}{2}\right)^2\tau_c{}^{\beta}}{C_\beta}\right)^k\frac{C_\alpha\tau_c{}^{\beta-1}t^{\beta+(\beta+1)k}}{C_\beta k!}\left(\frac{\Gamma[k+1]}{\Gamma[\beta+k(\beta+1)+1]}-\frac{C_\alpha\tau_c{}^{\beta-1}t^{\beta}\Gamma[k+2]}{C_\beta\Gamma[2\beta+k(\beta+1)+1]}\right). \tag{60}$$

Due to the fact that the three parameters Mittag-Leffler function isn't present in the special functions of Wolfram Mathematica, the Gamma Eulero function has been adopted into the code based on its definition.[44,45] This solution (60) is used to solve the problem for intermediate value of $\beta$ in the fractional photomechanical model, while the authors use Equations (61a) and (61b) to solve the particular solution of Equation (59) for $\beta=0$ and $\beta=1$, respectively.

$$p_1(t,z)=\frac{4}{\pi}\sum_{n=1}^{N}\frac{(-1)^n}{1-2n}\cos\left[\frac{(2n-1)\pi z}{2}\right]e^{-\frac{\left(\frac{(2n-1)\pi z}{2}\right)^2 t\tau_c}{C_\alpha+C_\beta\tau_c}}, \tag{61a}$$

$$g_1(t,z)=\frac{4}{\pi}\sum_{n=1}^{N}\frac{(-1)^n}{1-2n}\cos\left[\frac{(2n-1)\pi z}{2}\right]e^{-\frac{C_\alpha t}{2C_\beta}}\left(\cos\left[\frac{t\sqrt{4C_\beta\left(\frac{(2n-1)\pi z}{2}\right)^2\tau_c-C_\alpha{}^2}}{2C_\beta}\right]+\frac{C_\alpha\sin\left[\frac{t\sqrt{4C_\beta\left(\frac{(2n-1)\pi z}{2}\right)^2\tau_c-C_\alpha{}^2}}{2C_\beta}\right]}{\sqrt{4C_\beta\left(\frac{(2n-1)\pi z}{2}\right)^2\tau_c-C_\alpha{}^2}}\right). \tag{61b}$$

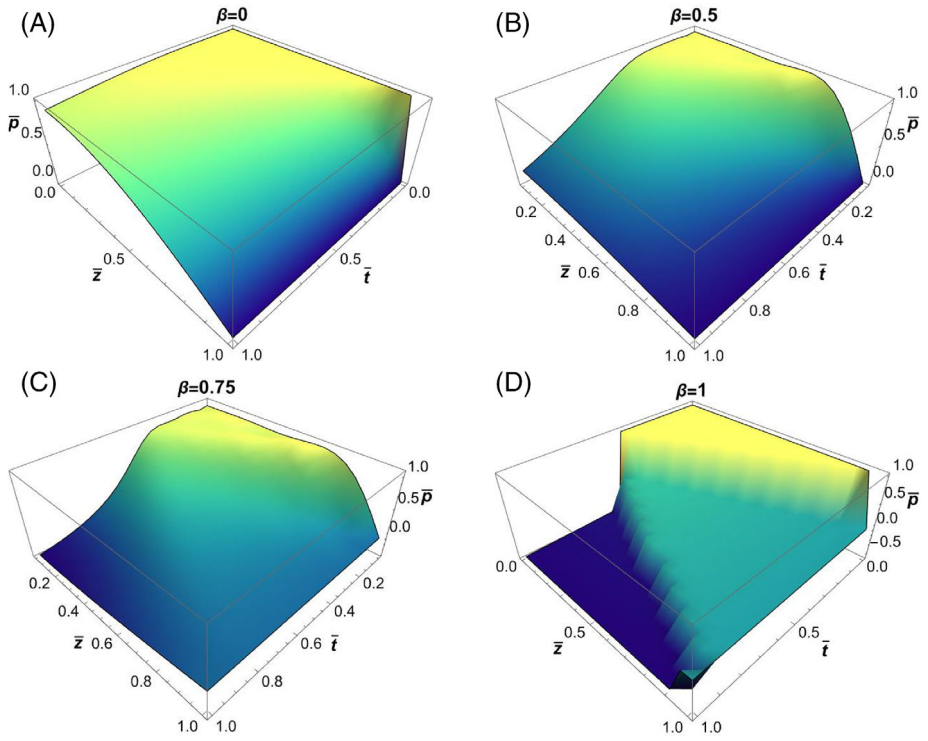


**FIGURE 4** Three-dimensional representation of non-dimensional pressure field $\bar{p}$ in the confined compression test for $\beta=0$, $\beta=0.5$, $\beta=0.75$, and $\beta=1$, in (A–D), respectively.

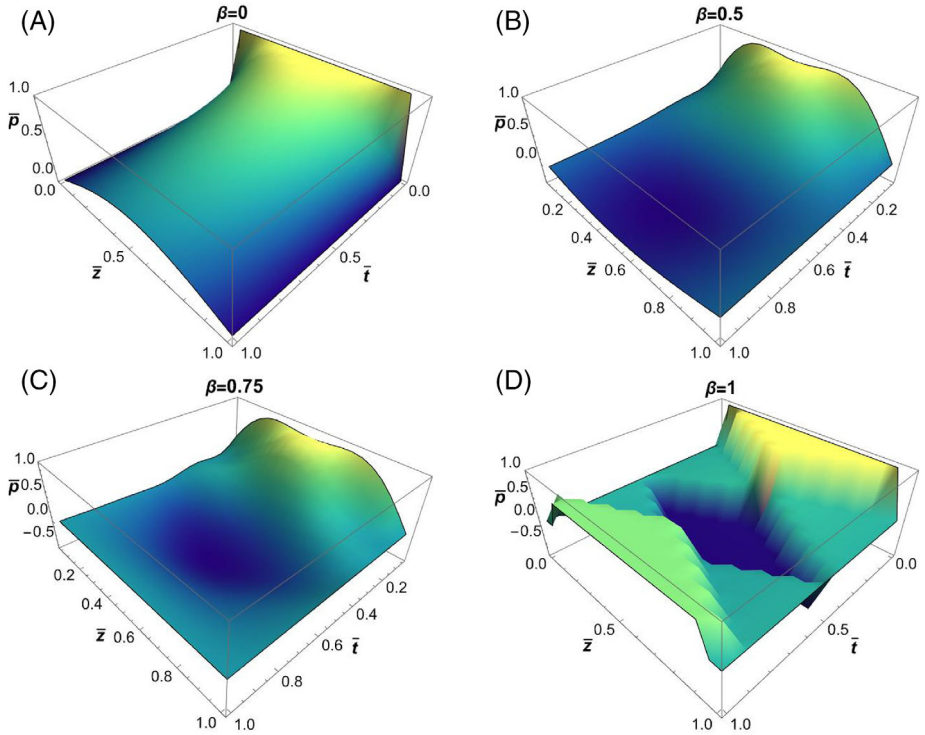


**FIGURE 5** Three-dimensional representation of non-dimensional pressure field $\bar{p}$ for various $\beta$ values in the fully drained case, particularly: $\beta = 0$ in (A), $\beta = 0.5$ in figure (B), $\beta = 0.75$ in (C), and $\beta = 1$ in (D).

Consequently, below there are the 3D graphs that highlight the relationship between the three parameters considered: dimensionless time $\bar{t}$, dimensionless height inside the cylinder $z$ and order of the fractional derivative $\beta$ (see Figure 4).

## 4.2 | Fully drained condition

The fully draining case has been analyzed in this section. Considering Equation (54), only the boundary conditions change because in this case water cannot escape laterally, through the bottom or the top surface, so:

$$\begin{cases} p(1,t) = \phi(1)y(t) = \phi(1) = 0 \\ p(0,t) = \phi(0y(t)) = \phi(0) = 0 \end{cases}. \tag{62}$$

It implies that $D_1 = 0$ and $sin(\lambda) = 0 \rightarrow \lambda_n = (2n-1)\pi; with\ n = 1,2,3.....$ So, Equation (48b) becomes, trivial solution excluded,

$$\phi(\bar{z}) = D_2 \sin(\lambda_n \bar{z}). \tag{63}$$

Similarly, the non-dimensional time problem remains unchanged as well as Equation (52) is still a solution of Equation (48b). Consequently,

$$\bar{p}(\bar{z},\bar{t}) = \sum_{n=1}^{\infty} D_n \sin(\lambda_n \bar{z}) y_n(\bar{t}) \tag{64}$$

is still a solution of Equation (46). Moreover, as done before, the orthogonality relations has been used to determine the coefficients $D_n$:

$$D_n = 2\int_0^1 \sin(\lambda_n \bar{z})d\bar{z} = \frac{4(-1)^{2n}}{\pi(2n-1)}. \tag{65}$$

Therefore, the general solution of the dimensionless problem is:

$$\begin{aligned}\bar{p}(\bar{z},\bar{t}) = &\frac{4}{\pi}\sum_{n=1}^{\infty}\frac{(-1)^{2n}}{2n-1}\sin(\lambda_n\bar{z})\sum_{k=0}^{\infty}\left(-\frac{\lambda_n^2}{\bar{C}_\beta}\right)^k\frac{\bar{t}^{k(\beta+1)}}{k!}E^k_{\beta,k(\beta+1)+1}\left(-\frac{C_\alpha}{\tau_c\bar{C}_\beta}\bar{t}^\beta\right)+\\ &+\frac{C_\alpha}{\tau_c\bar{C}_\beta}\sum_{k=0}^{\infty}\left(-\frac{\lambda_n^2}{\bar{C}_\beta}\right)^k\frac{\bar{t}^{k(\beta+1)+\beta}}{k!}E^k_{\beta,k(\beta+1)+1+\beta}\left(-\frac{C_\alpha}{\tau_c\bar{C}_\beta}\bar{t}^\beta\right).\end{aligned} \tag{66}$$

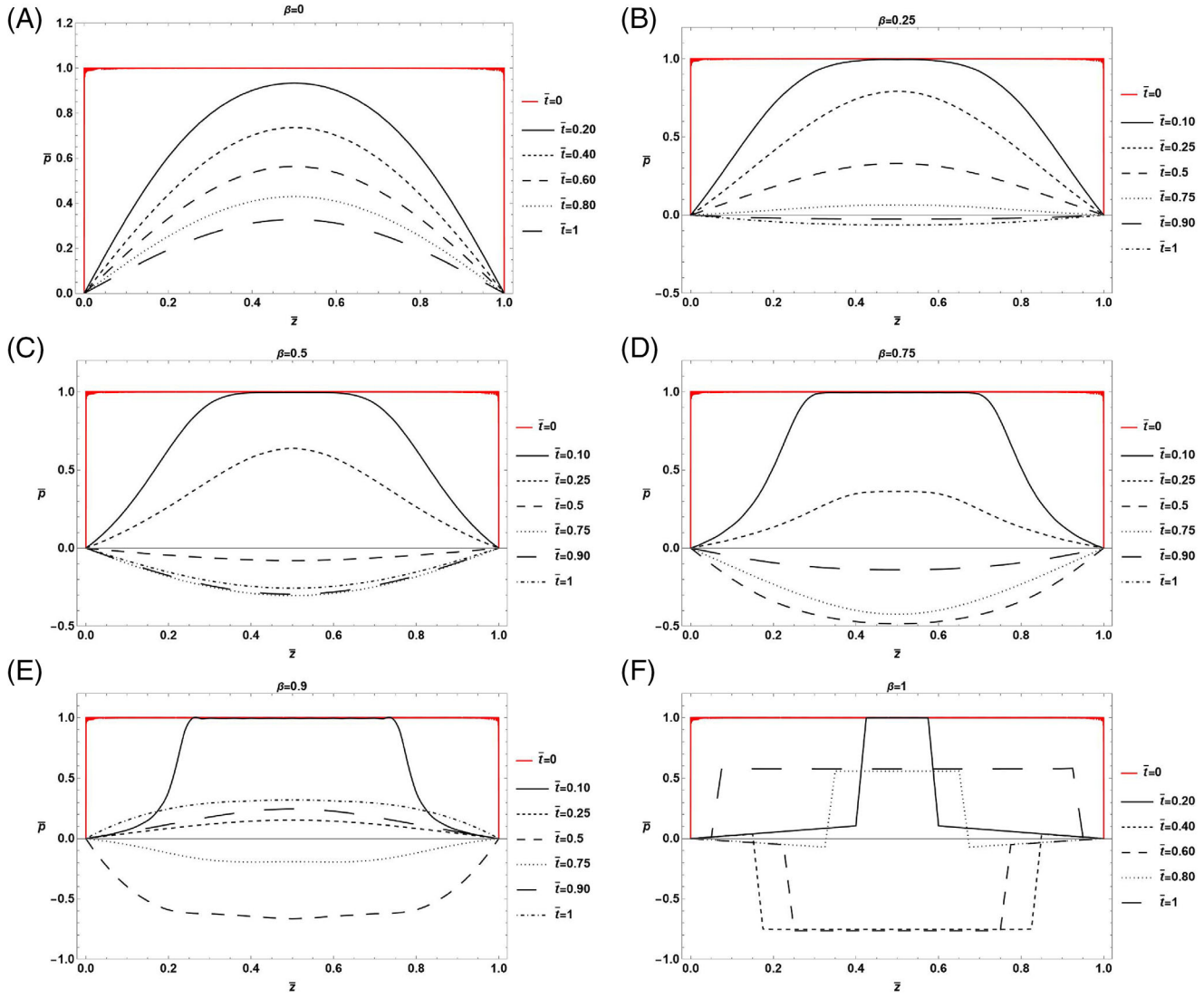


**FIGURE 6** Non-dimensional pressure field $\bar{p}$ for different values of $\beta$ in the confined compression test in the fully drained case, in detail: $\beta = 0$ (A), $\beta = 0.25$ (B), $\beta = 0.5$ (C), $\beta = 0.75$ (D), $\beta = 0.9$ (E), and $\beta = 1$ (F). Each curve represents the pressure field for a specific value of non-dimensional time $\bar{t}$, particularly the red line represents the confined compression test at the initial time that is, $\bar{t} = 0$.

Looking Equations (66) and (59), it can be seen that these solutions are very similar. The only significant difference is related to the coefficients $D_n$ and to the non-dimensional space solution $\phi(\bar{z})$. Particularly, there is the cosine function of $\bar{z}$ in the first case, and the sine function in the second one. Anyway, the non-dimensional time solution $y_n(\bar{t})$ is still the same in both cases.

As done before, Equation (66) has been implemented into Wolfram Mathematica, using Equation (67a) for intermediate value of $\beta$, and Equation (67b) and Equation (67c) for beta equals to zero and one, respectively.

$$f_2(\beta,\mathrm{t},\mathrm{z}) = \frac{4}{\pi}\sum_{n=1}^{N}\frac{(-1)^{2n}}{2n-1}\sin[(2n-1)\pi z]\sum_{k=0}^{100}\left(-\frac{((2n-1)\pi z)^2\tau_c{}^{\beta}}{C_\beta}\right)^k\frac{t^{(\beta+1)k}}{k!}\left(\frac{\Gamma[k+1]}{\Gamma[k(\beta+1)+1]}-\frac{C_\alpha\tau_c{}^{\beta-1}t^{\beta}\Gamma[k+2]}{C_\beta\Gamma[\beta+k(\beta+1)+1]}\right)$$
$$+\left(-\frac{((2n-1)\pi z)^2\tau_c{}^{\beta}}{C_\beta}\right)^k\frac{C_\alpha\tau_c{}^{\beta-1}t^{\beta+(\beta+1)k}}{C_\beta k!}\left(\frac{\Gamma[k+1]}{\Gamma[\beta+k(\beta+1)+1]}-\frac{C_\alpha\tau_c{}^{\beta-1}t^{\beta}\Gamma[k+2]}{C_\beta\Gamma[2\beta+k(\beta+1)+1]}\right), \tag{67a}$$

$$p_2(\mathrm{t},\mathrm{z}) = \frac{4}{\pi}\sum_{n=1}^{N}\frac{(-1)^{2n}}{2n-1}\sin[(2n-1)\pi z]e^{-\frac{((2n-1)\pi z)^2 t\tau_c}{C_\alpha+C_\beta\tau_c}}, \tag{67b}$$

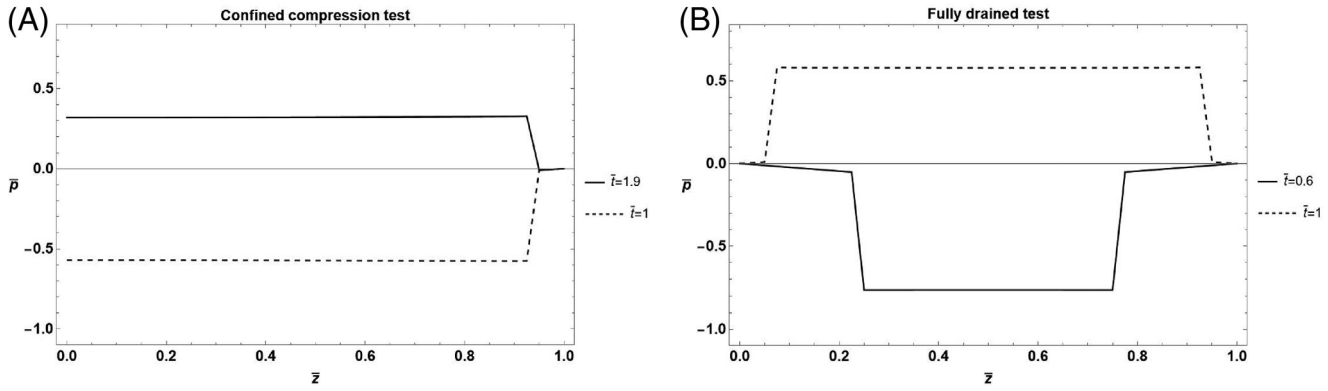


**FIGURE 7** Comparison of the non-dimensional pressure field $\bar{p}$ for $\beta = 1$ between the confined case (A) and the fully drained case (B), fixing the $\bar{t}$ value. In detail, dotted line is related to $\bar{t} = 1$, while continuous line is related to the time when pressure reach the opposite value that is, pressure reaches the negative value when $\bar{t} = 1.9$ in the confined compression test, while pressure is still positive when $\bar{t} = 0.6$ in the fully drained test.

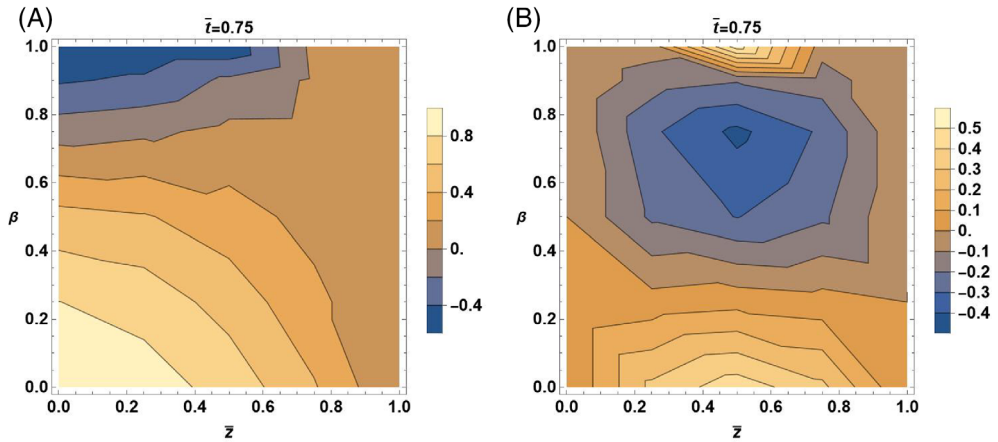


**FIGURE 8** Comparison of the non-dimensional pressure field $\bar{p}$ between the confined case (A) and the fully drained case (B), fixing the value of non-dimensional time $\bar{t} = 0.75$.

$$g_2(t,z)=\frac{4}{\pi}\sum_{n=1}^{N}\frac{(-1)^{2n}}{2n-1}\sin[(2n-1)\pi z]e^{-\frac{C_\alpha t}{2C_\beta}}\left(\cos\left[\frac{t\sqrt{4C_\beta((2n-1)\pi z)^2\tau_c-C_\alpha{}^2}}{2C_\beta}\right]+\frac{C_\alpha\sin\left[\frac{t\sqrt{4C_\beta((2n-1)\pi z)^2\tau_c-C_\alpha{}^2}}{2C_\beta}\right]}{\sqrt{4C_\beta((2n-1)\pi z)^2\tau_c-C_\alpha{}^2}}\right). \quad (67c)$$

Their numerical applications for various value of $\beta$ are shown into Figure 5. Meanwhile, Figure 6 shows the trend of non-dimensional pressure $\bar{p}$ for fixing non-dimensional time $\bar{t}$.

It can be seen that the time evolution of the pressure is strongly influenced by the order of Caputo's fractional derivative. The deviation from elastic behavior that is, $\beta=0$, has been revealed in the rapid pressure reduction in both time and space: this effect becomes more pronounced as the deviation from elastic behavior increases that is, $\lim_{\beta\to1}$. In all cases, as time increases the pressure value decreases, but anomalous porous media require shorter non-dimensional times than classical one (Figures 4A, 5A) to reach stability. In addition, observing the confined compression test (see Section 4.1), it is interesting to note that the non-dimensional pressure gradually decreases when $\beta<0.5$; on the other side, when $\beta\geq0.5$, a fast pressure drop is observed from 1 to 0 (see Figure 4). Moreover, in the last case, the pressure moves to negative values, too (Figure 3D–F). As $\beta$ increase, the $\bar{z}$ value of which it occurs decrease due to the fact that the hereditary material drives far and far from the elasticity. On the other hand, observing the fully drained test (see Section 4.2), the pressure just moves to negative values for a smaller value of $\beta$ that is, $\beta=0.25$ (see Figure 6B). Moreover, when $\beta=1$ and $\bar{t}\geq0.60$, the non-dimensional pressure returns to positive values, but lower than initial values (see Figure 6F). In the confined compression test, it happens for a greater value of $\bar{t}$ that is, only when $\bar{t}\geq1.9$, as shown in Figure 7.

In general, the solution's dependence on the $\beta$ value is greater in the drained case than in the confined case. As further confirmation, if we compare the pressure trend for the same value of $\bar{t}$, a greater part of porous medium has a negative value of $\bar{p}$ in the fully drained test, as shown in Figure 8.

## 5 | CONCLUSIONS

In this paper, the authors investigated the poromechanics of an hereditary porous media completely filled by a fluid modelling the biomechanics of the meniscus in the articular knee joint. The effects of the material hereditariness has been accounted for with the aid of fractional differential calculus extending the three axial constitutive equation of fractional-order hereditariness to include the fluid pressure field effect to describe the phenomenon of fluid diffusion in porous media.

The main result of this study, the effect of overpressure caused by the beta-order variability of the constitutive equation has been reported. It has been shown that overpressure in the tissue due to loading condition is strongly dependent on the order of Caputo's fractional derivative: higher is the order of $\beta$, faster has the pressure decreased. This aspect may be a leading issue in prediction of damages of menisci that may be favored by a slow release of the overpressure in presence of repetitive loads. Indeed the phenomenon of swelling and consolidation occurs when $\beta\geq0.5$ in the confined compression test, and for $\beta\geq0.25$ in the fully drained test.

In addition, as $\beta\neq0$, it has been shown that the overpressure reaches negative values and then returns to positive values when the value of non-dimensional time increases. This effect is interesting since no literature evidence of an oscillating pressure field has been uncovered by the use of classical mathematical modelling to represent the material hereditariness.

Experimental campaign reporting data on the hereditary behavior of the menisci as well as on pressure drops in confined compression tests is underway and it will be reported elsewhere.

The model lays the foundations for a more accurate analysis of the poromechanical modeling of the meniscus. In fact, the fractional derivative, as well known in the literature,[3,13,36] is able to well describe the highly viscoelastic behavior of biological tissues and the effects due to the aqueous matrix. The model should be implemented and integrated into subroutines in finite element software. It would become a predictive model of the behavior of the meniscus over time and would provide an additional tool for the creation of a meniscus prosthesis, which is still not a solution available to orthopedic surgeons today.

## ACKNOWLEDGMENTS

The authors are very grateful to "PON FSE-FESR ricerca e innovazione 2014-2020DOT1320558" (Ms Fabiana Amiri) and to "Progetti DM 1062 del 10/08/2021 (Ricercatori a tempo Determinato tipo A (RTDA)) n. grant 20-I-39045-8"

(Dr. Emanuela Bologna). The authors thank the projec SiciliAn MicronanOTecH Research And Innovation CEnter SAMOTHRACE (MUR, PNRR-M4C2, ECS00000022), spoke 3: Università degli Studi di Palermo "S2-COMMs-Micro and Nanotechnologies for Smart & Sustainable Communities".

## DATA AVAILABILITY STATEMENT

Data sharing not applicable to this article as no datasets were generated or analysed during the current study.

## ORCID

*Fabiana Amiri* https://orcid.org/0000-0001-6293-8932
*Massimiliano Zingales* https://orcid.org/0000-0001-9093-9529

## REFERENCES

1. Mcdermott ID, Amis AA. The consequences of meniscectomy. *Bone Jt J*. 2006;88(12):1549-1556.
2. Fox AJS, Wanivenhaus F, Burge AJ, Warren RF, Rodeo SA. The human meniscus: A review of anatomy, function, injury, and advances in treatment. *Clin Anat*. 2015;28:269-287.
3. Barrera O, Bologna E, Zingales M, Alotta G. Experimental characterization of the human meniscal tissue. Proceedings of the International Forum on Research and Technologies for Society and Industry Innovation to shape the future. 2018.
4. Imeni M, Seyfi B, Fatouraee N, Samani A. Constitutive modeling of menisci tissue: a critical review of analytical and numerical approaches. *Biomech Model Mechanobiol*. 2020;19:1979-1996.
5. Mansour JM. Biomechanics of cartilage. *Kinesiol Mech Pathomechanics Hum Mov*. 2nd ed. 2013:69-83. https://web.mit.edu/cortiz/www/3.052/3.052CourseReader/27_BiomechanicsofCartilage.pdf
6. Moroni L, Lambers FM, Wilson W, et al. Finite element analysis of meniscal anatomical 3D scaffolds: implications for tissue engineering. *Open Biomed Eng J*. 2007;1:23-34.
7. Caputo M. Models of flux in porous media with memory. *Water Resour Res*. 2000;36:693-706.
8. Caputo M, Plastino W. Diffusion in porous layers with memory. *Geophys Int J*. 2004;158:385-396.
9. Uzuner S, Li LP, Kucuk S, Memisoglu K. Changes in knee joint mechanics after medial meniscectomy determined with a poromechanical model. *J Biomech Eng*. 2020;142(10):101006.
10. Deseri L, Zingales M. A mechanical picture of fractional-order Darcy equation. *Commun Nonlinear Sci Numer Simul*. 2015;20(3):940-949.
11. Alaimo G, Piccolo V, Cutolo A, Deseri L, Fraldi M, Zingales M. A fractional order theory of poroelasticity. *Mech Res Commun*. 2019;100:103395.
12. Bologna E, Graziano F, Deseri L, Zingales M. Power-laws heredinariness of biomimetic ceramics for cranioplasty. *Int J Non-Linear Mech*. 2019;115:61-67.
13. Bologna E, Di Paola M, Dayal K, Deseri L, Zingales M. "Fractional-order nonlinear hereditariness of tendons and ligaments of the human knee." Phyl. *Tran R Soc A: Math Phys Eng Sci*. 2020;378(2172):20190220.
14. Maes JA, Donahue TH. Time dependent properties of bovine meniscal attachments: stress relaxation and creep. *J Biomech*. 2006;39(16):3055-3061.
15. Norberg C, Filippone G, Andreopoulos F, et al. Viscoelastic and equilibrium shear properties of human meniscus: Relationships with tissue structure and composition. *J Biomech*. 2021;120:110343.
16. Camarda L, Bologna E, Pavan D, et al. Posterior meniscal root repair: a biomechanical comparison between human and porcine menisci. *Muscles Ligaments Tendons J*. 2019;9(1):76-81.
17. Palumbo FS, Fiorica C, Pitarresi G, Zingales M, Bologna E, Giammona G. Multifibrillar bundles of a self-assembling hyaluronic acid derivative obtained through a microfluidic technique for aortic smooth muscle cell orientation and differentiation. *Biomater Sci*. 2018;6(9):2518-2526.
18. Ionescu C, Lopes A, Copot D, Machado JAT, Bates JHT. The role of fractional calculus in modeling biological phenomena: a review. *Commun Nonlinear Sci Numer Simul*. 2017;51:141-159.
19. Carpinteri A. *Fractals and Fractional Calculus in Continuum Mechanics*. Springer-Verlag; 1997. doi:10.1007/978-3-7091-2664-6
20. Nutting P. A new general law of deformation. *J Frankl Inst*. 1921;191(5):679-685.
21. Di Paola M, Pirrotta A, Valenza A. Visco-elastic behavior through fractional calculus: an easier method for best fitting experimental results. *Mech Mater*. 2011;43(12):799-806.
22. Bologna E, Zingales M, Alotta G, Deseri L. Quasi-fractional models of human tendons hereditariness. Proceedings of the IEEE 4th International Forum on Research and Technologies for Society and Industry. 2018.
23. Deseri L, Di Paola M, Zingale M, Polacci P. Power-law hereditariness of hierarchical fractal bones. *Int J Numer Methods Eng*. 2016;29:1338-1360.
24. Sun HG, Zhang Y, Baleanu D, Chen W, Chen YQ. A new collection of real world applications of fractional calculus in science and engineering. *Commun Nonlinear Sci Numer Simul*. 2018;64:213-231.
25. Caputo M, Cametti C. Fractional derivatives in the diffusion process in heterogeneous systems: The case of transdermal patches. *Math Biosci*. 2017;291:38-45.

26. Zingales M. An exact thermodynamical model of power-law temperature time scaling. *Ann Phys*. 2016;365:24-37.
27. Marchiorri G, Lopomo NF, Bologna E, et al. How preconditioning and pretensioning of grafts used in ACLigaments surgical reconstruction are influenced by their mechanical time-dependent characteristics: Can we optimize their initial loading state? *Clin Biomech*. 2021; 83:105294.
28. Alotta G, Bologna E, Failla G, Zingales M. A fractional approach to non-newtonian blood rheology in capillary vessels. *J Per NLoc Mod*. 2019;1:88-96.
29. Bologna E, Di Paola M, Zingales M. A single integral approach to fractional order non-linear hereditariness. *Lect Notes in Mech Eng*. 2020;932-944.
30. Dinoto E, Mirabella D, Ferlito F, et al. Carotid artery disease in the era of biomarkers: a pilot study. *Diagnostics*. 2023;13(4):644.
31. Bologna E, Di Paola M, Zingales M. A Single Integral Approach to Fractional Order Non-Linear Hereditariness. In: Carcaterra, A., Paolone, A., Graziani, G. (eds), *Proceedings of XXIV AIMETA Conference 2019. AIMETA 2019. Lecture Notes in Mechanical Engineering*. Springer; 2020. doi:10.1007/978-3-030-41057-5_76
32. Alotta G, Bologna E, Zingales M. Exact mechanical hierarchy of non-linear fractional-order hereditariness. *Symmetry*. 2020;12(4):673.
33. De Caro V, Murgia D, Seidita F, et al. Enhanced in situ availability of aphanizomenon flos-aquae constituents entrapped in buccal films for the treatment of oxidative stress-related oral diseases: biomechanical characterization and in vitro/ex vivo evaluation. *Pharmaceutics*. 2019;35.
34. Dintcheva NT, Baiamonte M, Teresi R, Alotta G, Bologna E, Zingales M. A fractional-order model of biopolyester containing naturally occurring compounds for soil stabilization. *Ad Mater Sci Eng*. 2019;882-889.
35. Mino GD, Airey G, Di Paola M, Pinnola FP, D'Angelo G, Presti DL. Linear and nonlinear fractional hereditary constitutive laws of asphalt mixtures. *J Civ Eng Manag*. 2016;22(7):882-889.
36. Bologna E, Lopomo N, Marchiori G, Zingales M. A non-linear stochastic approach of ligaments and tendons fractional-order hereditariness. *Prob Eng Mech*. 2020;60:103034.
37. Alotta G, Barrera O, Cocks A, Di Paola M. The numerical implementation of a 3D fractional viscoelastic constitutive model. *Finite Elem Anal Des*. 2015;193:1-13.
38. Mainardi F, Spada G. Creep, relaxation and viscosity properties for basic fractional models in rheology. *Eur Phys J Spec Top*. 2011; 193(1):133-160.
39. Biot MA. General theory of three dimensional consolidation. *J Appl Phys*. 1941;12:155-164.
40. Pinsky MA. Partial differential equations and boundary-value problems with applications: third edition. *Pure and Applied Undergraduate Texts*. 1998;15:526.
41. Podlubny I. Fractional differential equations. *Math Sci Eng*. 1999;204:198.
42. Srivastava HM, Srivastava HM, Trujillo JJ. Theory and applications of fractional differential equations. *North-Holland Math Stud*. 2006;198.
43. Diethelm K. The analysis of fractional differential equations. *Lect Notes Math*. 2010;2004:1-51.
44. Haubold HJ, Mathai AM, Saxena RK. Mittag-leffler functions and their applications. *J Appl Math*. 2011;1–51:1-51.
45. Sen GI, Debnath L. Some properties of the Mittag-Leffler functions. *Integral Transf Special Funct*. 2007;18:329-336.
46. Iaffaldano G, Caputo M, Martino S. Experimental and theoretical memory diffusion of water in sand. *Hydrol Earth Syst Sci Discuss*. 2005;2(4):1329-1357.


**How to cite this article:** Amiri F, Bologna E, Nuzzo G, Moroni L, Zingales M. Fractional-order poromechanics for a fully saturated biological tissue: Biomechanics of meniscus. *Int J Numer Meth Biomed Engng*. 2023;39(11): e3732. doi:10.1002/cnm.3732